Pergamon

Journal of Structural Geology, Vol. 17, No. 11, pp. 1601 to 1613, 1995

0191-8141/95 $9.50+0.00

0191-8141(95)00047-X

Control of magnetic rock fabrics by mica preferred orientation: a quantitative approach

SIEGFRIED SIEGESMUND

Institut für Geologie und Dynamik der Lithosphäre, 37077 Göttingen, Germany

KLAUS ULLEMEYER

Joint Institute of Nuclear Research, Frank Laboratory for Neutron Physics, 141980 Dubna, Russia

and

MICHAEL DAHMS

GKSS Forschungszentrum Geesthacht GmbH, 21502 Geesthacht, Germany

(*Received* 10 *November* 1993; *accepted in revised form* 18 *April* 1995)

Abstract—Magnetic anisotropy analysis represents a well-established and frequently used method in structural geology. Several attempts were made to relate the anisotropy of magnetic susceptibility (AMS) to rock fabrics and to discover the sources of the AMS. In gneissic rocks, paramagnetic phyllosilicates with lattice-dependent magnetic properties are assumed to control the whole rock AMS, i.e. it is dominated by mica lattice preferred orientation (texture). In this study, AMS was modelled on the basis of the mica texture, the rock composition and compared to the experimentally determined AMS. The orientations of the modelled and experimental tensors agree quite well, whereas all the other characteristic parameters (shape, anisotropy, mean susceptibility) display large differences. It has been concluded that accessory high susceptible phases, as well as the diamagnetic rock constituents, may have significant influence on AMS. Consequently, mica pole figure measurements cannot be replaced by AMS measurements without control of the sources of AMS. It was also concluded, that the March model to evaluate strain from mica-preferred orientations is not valid for highly strained rocks. Beside the fact that the obtained strains are too low, the deformation is generally inhomogeneous, which leads to an overprint of the mica texture. Since the microstructural fabric elements which originate in different strain regimes (prolate or oblate) may create similar modifications of the mica orientation patterns, it is obvious that the relationship between AMS and deformation is rather complex.

INTRODUCTION

Magnetic susceptibility K is an intrinsic and often anisotropic physical property of rock-forming minerals. Consequently, the resulting magnetic susceptibility of a rock is also anisotropic. This holds true for sedimentary, magmatic and metamorphic rocks as well. In polyphase rocks that occur commonly in nature, the mean susceptibility $\bar{K}$ is the sum of the individual contributions of each dia-, para- and ferromagnetic mineral with respect to its volume fraction. Anisotropy of magnetic susceptibility (AMS) is dependent on several parameters: mineralogical composition (e.g. Borradaile *et al.* 1987), single crystal anisotropy (Hrouda 1982), grain shape (Uyeda *et al.* 1963) and lattice preferred orientation (Owens & Rutter 1978, Hrouda *et al.* 1985). Ferromagnetic magnetite is the only mineral in which AMS mainly depends on grain shape, in all other important anisotropic (generally paramagnetic) minerals it is controlled by lattice preferred orientation (see Borradaile 1988 for discussion).

Recently, the AMS has been accepted as a method for the measurement of fabric in deformed rocks. This was initiated by the observation that in many rocks accessory ferromagnetic minerals do not control the bulk rock AMS. In contrast to earlier findings it could be shown by Rochette (1987), that generally paramagnetic minerals are responsible for bulk rock AMS. For example, in gneissic rocks with the main constituents quartz, plagioclase, K-feldspar and mica minerals, the shape of the AMS tensor is controlled by the paramagnetic phyllosilicates (the only anisotropic phase). Furthermore, it can be deduced, that the orientation of its principal axes $\vec{K}_{max}$, $\vec{K}_{int}$, $\vec{K}_{min}$ often coincide with macroscopic fabric elements. The $\vec{K}_{max}\vec{K}_{int}$ plane (magnetic foliation) parallels the rock foliation (schistosity, metamorphic banding, magmatic layering, mylonitic foliation), whereas $\vec{K}_{min}$ parallels the foliation pole. In most cases $\vec{K}_{max}$ is subparallel to the mineral or stretching lineation. A wealth of qualitative and quantitative data is presented in the literature which discusses the source of AMS and the relationship between the AMS ellipsoid and the finite strain ellipsoid. For a recent review refer to Borradaile (1988, 1991).

Until recently, modelling of rock AMS was mostly restricted to the calculation of the orientation of the

AMS tensor from the orientation tensor of the phyllosilicate basal planes (Hrouda & Schulmann 1990, Richter *et al.* 1993a). Richter *et al.* (1993b) considered simplified three-phase systems composed of quartz, muscovite and hematite or magnetite to model the magnitude of bulk rock susceptibility. In the present paper, modelling was carried out by considering the composition of the rock to obtain the magnitude of rock susceptibility. From the phyllosilicate (001) pole figures provided by X-ray goniometry and U-stage measurements, a theoretical AMS-tensor (corresponding to a rock consisting of 100% phyllosilicates) was calculated and combined with the theoretical tensors of all present mineral phases according to their volume contents. The resulting tensor is then compared with the experimentally determined tensor. Modelling was applied to some selected metamorphic and mylonitic rocks representing a variety of metamorphic conditions, deformation history and a different degree of bulk strain. In view of the application of the AMS in structural geology, the general aspect of the relationship between the rock fabric and magnetic fabric will be discussed in this paper. Emphasis is placed on the question whether the fast and non-destructive AMS method is really able to describe the rock fabric, strain magnitude and the preferred orientation of minerals accurately.

THEORETICAL BACKGROUND

AMS tensor calculation from texture

Magnetic susceptibility K can be described by a second-rank tensor with non-zero components K_{ii} or by an ellipsoid. This tensor relates the intensity of the applied external field $\vec{H}$ to the acquired magnetization $\vec{M}$ of the material:

$$\vec{M} = K_{ii}\vec{H}. \tag{1}$$

In a single crystal, it is:

$$K(\vec{h}) = K_{11}h_1^2 + K_{22}h_2^2 + K_{33}h_3^2 \tag{2}$$

where $\vec{h}$ represents a crystal direction with the vector components h_i.

A mean value of the property $\bar{K}$ in a specific direction of a textured polycrystal $\vec{h}$ can be calculated as follows (Bunge 1982):

$$\bar{K}(\vec{y}) = \sum_{l=0}^{2} \sum_{\nu=1}^{N(l)} \bar{e}_l^{\nu} k_l^{\nu}(\vec{y}) \tag{3}$$

where k_l^{ν} are spherical harmonics satisfying sample symmetry and the integer $N(l)$ is defined by the sample symmetry. The coefficients $\bar{e}_l^{\nu}$ are calculated from the texture coefficients $C_l^{\mu\nu}$ by

$$\bar{e}_l^{\nu} = \frac{1}{2l+1} \sum_{\mu=1}^{M(l)} C_l^{\mu\nu} e_l^{\mu} \tag{4}$$

with the coefficients e_l^{μ}, which are determined from the tensor components K_{ii} (Bunge 1982):

$$e_0^1 = \frac{K_{11} + K_{22} + K_{33}}{3} \tag{5a}$$

$$e_2^1 = \sqrt{\frac{4\pi}{5}} \frac{2K_{33} - K_{11} - K_{22}}{3} \tag{5b}$$

$$e_2^2 = \sqrt{\frac{4\pi}{5}} \frac{K_{11} - K_{22}}{\sqrt{3}}. \tag{5c}$$

The integer $M(l)$ depends on the symmetry of the second order tensor. For $l = 0$, it is always 1. For $l = 2$, it is 2, but we can see that for $K_{11} = K_{22}$, i.e. axial symmetry, l_2^2 vanishes and for $K_{11} = K_{22} = K_{33}$, i.e. spherical symmetry, l_2^1 vanishes as well.

The coefficients are calculated from the measured pole figures (Bunge 1982). A special case is valid for our investigations and therefore should be addressed here: if a complete basal plane pole figure is available in a non-cubic polycrystal, the series coefficients $C_l^{l\nu}$ can be calculated directly from the pole figure coefficients $F_l^{\nu}(001)$ by:

$$C_l^{l\nu} = \sqrt{\frac{4\pi}{2l+1}} F_l^{\nu}(001). \tag{6}$$

In a distinct sample direction $\vec{y}$, the resulting magnetic susceptibility $\bar{K}_{\text{rock}}$ of a rock containing I different mineral phases is now the sum of all mineral susceptibilities weighted by their volume percentages V_i:

$$\bar{K}_{\text{rock}}(\vec{y}) = \sum_{i=1}^{I} V_i \bar{K}_i(\vec{y}). \tag{7}$$

According to the common usage in the AMS literature, $K_{11} = K_{\max}$, $K_{22} = K_{\text{int}}$ and $K_{33} = K_{\min}$ was set with the corresponding directions $\vec{K}_{\max}$, $\vec{K}_{\text{int}}$ and $\vec{K}_{\min}$.

AMS of a single crystal

An extensive literature exists on the characteristic parameters of the mineral mean susceptibility and anisotropy ratio (e.g. Hrouda 1982, Borradaile *et al.* 1987). Data about the orientation of the principal susceptibility axes with respect to the crystallographic axes are poor for most rock-forming minerals. These minerals are solid solutions with varying chemical composition which causes variations of all magnetic parameters of the single crystal.

In the considered rocks, biotite and muscovite are the only minerals with anisotropic magnetic properties (Table 1). Both are monoclinic with $\vec{K}_{\min}$ parallel to the crystallographic c-axis and $\vec{K}_{\text{int}}$ and $\vec{K}_{\max}$ lying in the basal plane (Fig. 1a). Zapletal (1990) confirmed the pseudohexagonal behaviour and the rotational symmetry of biotite. The mean susceptibilities for the mica group vary with composition; $\bar{K}$ for biotite is about eight times higher than for muscovite. For biotite and muscovite the data given by Borradaile *et al.* (1987) were used

Table 1. Mineral susceptibilities used for the performed calculations

	Ref.	K	K_{max}	K_{int}	K_{min}	K_{max}/K_{min}	Remarks	Assumptions.
Biotite	(1)	1180	1.098	1.095	0.832	1.32	$K_{max}\perp\langle c\rangle$ $K_{int}\perp\langle c\rangle$ $K_{min}\parallel\langle c\rangle$	$K_{max} = K_{int}$ $= 1.097$
Muscovite	(1)	165	1.159	1.052	0.820	1.41	$K_{max}\perp\langle c\rangle$ $K_{int}\perp\langle c\rangle$ $K_{min}\parallel\langle c\rangle$	$K_{max} = K_{int}$ $= 1.106$
Quartz	(2)	−13.4						
Plagioclase	(3)	−2.7						isotropic
K-feldspar	(4)	−12.0						

Data from (1) Borradaile *et al.* (1987), (2) Hrouda (1986), (3) Borradaile (1987) and (4) Finke (1910).

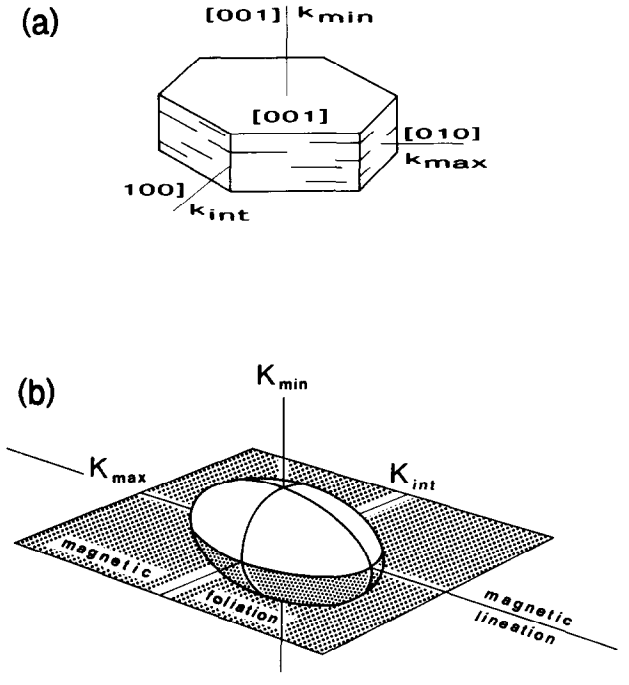

Fig. 1. (a) Relationship between the principal susceptibility axes $\vec{K}_{max}$, $\vec{K}_{int}$, $\vec{K}_{min}$ and the crystallographic axes [100], [010], [001] of mica minerals; (b) definition of the virtual fabric elements 'magnetic foliation' and 'magnetic lineation'.

for the calculations. The anisotropy of biotite in the basal plane is very low (K_{max}/K_{int} = 1.003), that of muscovite is much higher (K_{max}/K_{int} = 1.102). An axial symmetry can be obtained when neglecting the anisotropy in the case of biotite and assuming a random distribution for all directions other than (001) in the case of muscovite (K_{max} set equal to K_{int} and then replacing them by the mean value of the single crystal). The AMS can then be calculated from the pole figure coefficients $F_l^y(001)$ from a complete pole figure as shown above. Any physical interaction between single grains can be neglected. These minerals display magnetocrystalline anisotropy independent of the mineral shape, which is reasonably constant from grain to grain (see discussion in Hrouda & Schulmann 1990).

Quartz, plagioclase and K-feldspar are diamagnetic and exhibit only very small anisotropies (Finke 1910, Hrouda 1986). When calculating bulk rock AMS, an isotropic behaviour was assumed for these minerals.

EXPERIMENTAL METHODS

Measurement and representation of low-field AMS

AMS was measured with a KLY-2 Kappabridge (Geofyzika, Brno) and computed using the ANISO 11 program developed by Jelinek (1977). The principle of the Kappabridge and the measuring procedure are explained by Hrouda (1982). The output of the program are parameters of the AMS-ellipsoid (Fig. 1b), which is defined by the lengths of its semiaxes and its orientation with respect to the sample coordinate system. For representation, the parameters P' and T proposed by Jelinek (1981) are used, with P' characterizing the degree of anisotropy and T the shape of the AMS-tensor. The latter refers to an oblate ($T = +1$) and prolate ($T = -1$) AMS corresponding to a pancake- and cigar-shaped ellipsoid, respectively. Some advantages of these two parameters for tensor representation are discussed by Jelinek (1981). From each sample, a minimum of three standard size cores was measured in order to have some control on the quality of the measured data. In all P'/T diagrams mean values are given. Additionally, extreme values are indicated by horizontal and vertical bars to mark the scatter of the data (with the exception for samples OG 23 and OG 25). The orientation of the tensors is represented in the phyllosilicate pole figures by the average of all individual measurements, and any significant deviation is discussed in the text.

Texture analysis

X-ray pole figure measurements of mica (001) at a scattering angle of $\Theta \approx 4.5°$ ($Cu_{K\alpha}$ radiation) were conducted using a pole figure goniometer operating in backreflection mode. Generally two sections have been measured up to a pole angle of 70°, the first one parallel to the foliation, the second one perpendicular to the foliation and parallel to the stretching lineation (except for sample W96 where the pole figure shows a sharp point maximum close to the foliation pole; only the section parallel to the foliation was measured). After the background subtraction and defocusing correction (Ullemeyer & Weber 1994) the incomplete pole figures of the two sections were rotated, adapted in intensity level and combined. To obtain the complete pole fig-

Table 2. Modal composition of the investigated rock samples obtained from quantitative X-ray analysis (SZx) or point counting (others)

Sample	Mica	Quartz	Plagioclase	K-feldspar
OG23	14*	45	26	15
OG25	14*	45	26	15
W13	7*	42	12	39
W41	7*	35	22	36
W96	14*	45	26	15
SZ12	32†	29	23	16
SZ21	32†	29	23	16
SZ41	32†	29	23	16

*Biotite.
†Muscovite.

ures, the missing part was calculated by interpolation, assuming that it contains no important textural information. The corrected intensities were normalized to express densities as multiples of random distribution (m.r.d.) and plotted in the lower hemisphere, equal area projection. The plane of projection is the main foliation, the stretching lineation is oriented horizontal, except for sample W41.

Mica (001) cleavage planes of the orthogneiss samples OG23 and OG25 were measured in three mutually perpendicular thin sections on a U-stage. After rotation onto the projection plane, pole density distributions of the (001) normals were calculated from the single grain data using the algorithm described by Adam (1989).

Since (001) mica-preferred orientations are generally characterized by orthorhombic or higher symmetry, they may be described by the orientation tensor (Scheidegger 1965) without loss of information. The principal directions of the orientation tensor ($\vec{e}_{min}, \vec{e}_{int}, \vec{e}_{max}$) are given in the pole figures for a better comparison with the experimental AMS tensor. According to the definition of Jelinek (1981), its shape is also characterized by the shape factor T_{mica}. Since mica is the only anisotropic mineral phase for AMS modelling, the principal directions of the orientation tensor correspond to the principal directions of the modelled AMS tensor. From the single crystal anisotropies of mica minerals, the following analogies may be deduced: $\vec{e}_{min}$ parallels $\vec{K}_{max}$, $\vec{e}_{int}$, parallels $\vec{K}_{int}$, $\vec{e}_{max}$ parallels $\vec{K}_{min}$.

SAMPLE DESCRIPTION

Orthogneiss samples (*OG23*, *OG25*)

Both samples (Bartosek *et al.* 1985, Siegesmund *et al.* 1993) of this group have (Table 2) an identical mineralogical composition (plagioclase, K-feldspar, quartz, biotite) and accessoric minerals (sillimanite, muscovite, apatite, ilmenite), but display different microfabrics related to different positions within a large-scale fold structure. OG23 (limb area) has pronounced foliation(s), which is defined by a compositional banding of alternating quartz/feldspar and mica-rich layers. The macroscopically visible lineation (L_1) is represented by rods of quartz/feldspar and biotite. In sections cut perpendicular to L_1 and S, two additional sets of subordinate foliations inclined about 40° to the main foliation can be observed. In sections parallel to the lineation the strongly developed planar fabric results from the superposition of these different foliations. The dominant foliation in OG25 (hinge zone) is microfolded around the crenulation axis (L_2) where L_2 is oriented perpendicular to L_1 in OG23. Beside the reorientation parallel to the crenulated layers, individual mica plates which are homogenously distributed within the rock matrix show a corresponding preferred orientation parallel to the limbs of the crenulated microfolds (see Figs. 2a & b).

Progressively deformed mylonite sequence (*SZ12*, *SZ21*, *SZ41*)

The metagranitoid complex within the Sesia Lanzo Zone (Isler and Zingg 1974, Compagnoni 1977) near the Insubric Line is strongly deformed. For this study, three rock samples (Table 2) were selected which have been progressively deformed from metagranitoid to mylonite and ultramylonite. These rocks contain mineral assemblages of a high pressure/low temperature metamorphism which represent relicts due to a retrograde overprinting under greenschist facies conditions. The metagranitoid (SZ12) shows a very weakly developed foliation which is macroscopically visible as flattened quartz crystals. The prolate grains are oriented with their long axes parallel to the lineation. SZ21 is a L-tectonite where the stretching lineation is defined by elongated quartz rods. Quartz shows typical intracrystalline deformation structures. The ultramylonite SZ41 (Figs. 2c & d) exhibits a pronounced mylonitic foliation. The macroscopically developed lineation is represented by quartz and plagioclase rods.

Granulites (*W96*, *W41*, *W13*)

The acid granulites from the Moldanubian zone in Lower Austria are mainly composed of quartz, orthoclase, plagioclase, biotite, sillimanite and garnet (Table 2). All the samples were collected in strongly deformed granulite lenses or layers incorporated in shear zones, which originated during nappe thrusting in the Moldanubian zone at Hercynian time. The granulites are interpreted as high temperature mylonites which obtained their fabric under dry upper amphibolite facies conditions (Weber & Duyster 1991). Common to all the samples is a strong foliation, but a pronounced stretching lineation is present only in sample W13. In contrast, sample W96 (Figs. 2e & f) displays no macroscopically visible linear fabric element, but the c-axes of prismatic sillimanite needles show a strong preferred orientation (sharp point maximum in the foliation) clearly defining the direction of maximum elongation (Ullemeyer 1992). In sample W41, two weak lineations are developed, but the stretching direction could be identified on polished

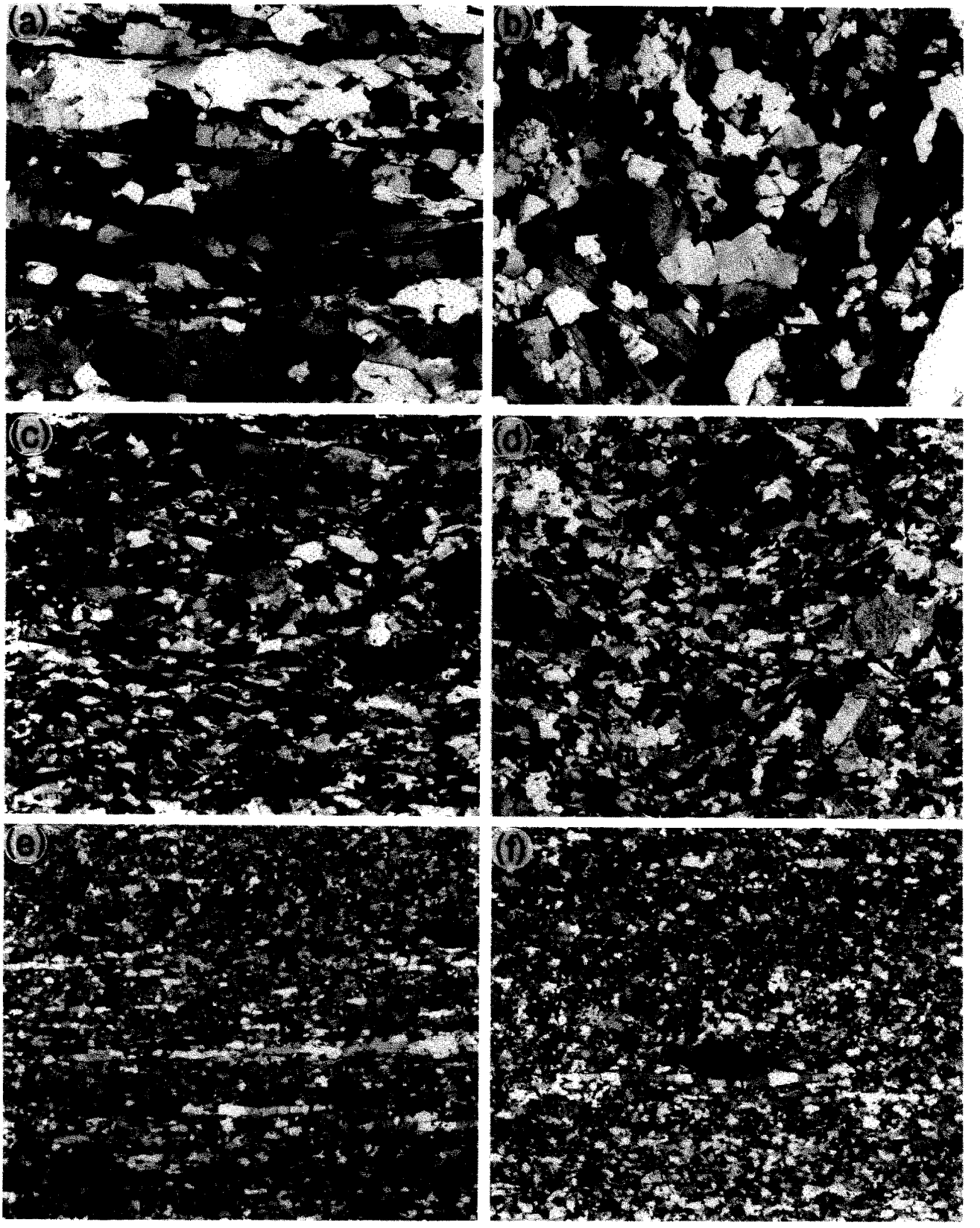

Fig. 2. Photomicrographs of rock fabrics in sections perpendicular to S and parallel to L (a, c, e), and perpendicular to S and perpendicular to L (b, d, f) for orthogneiss OG25 (a) & (b), the ultramylonite SZ41 (c) & (d) and the granulite W96 (e) & (f). Oblique-crossed polarized light.

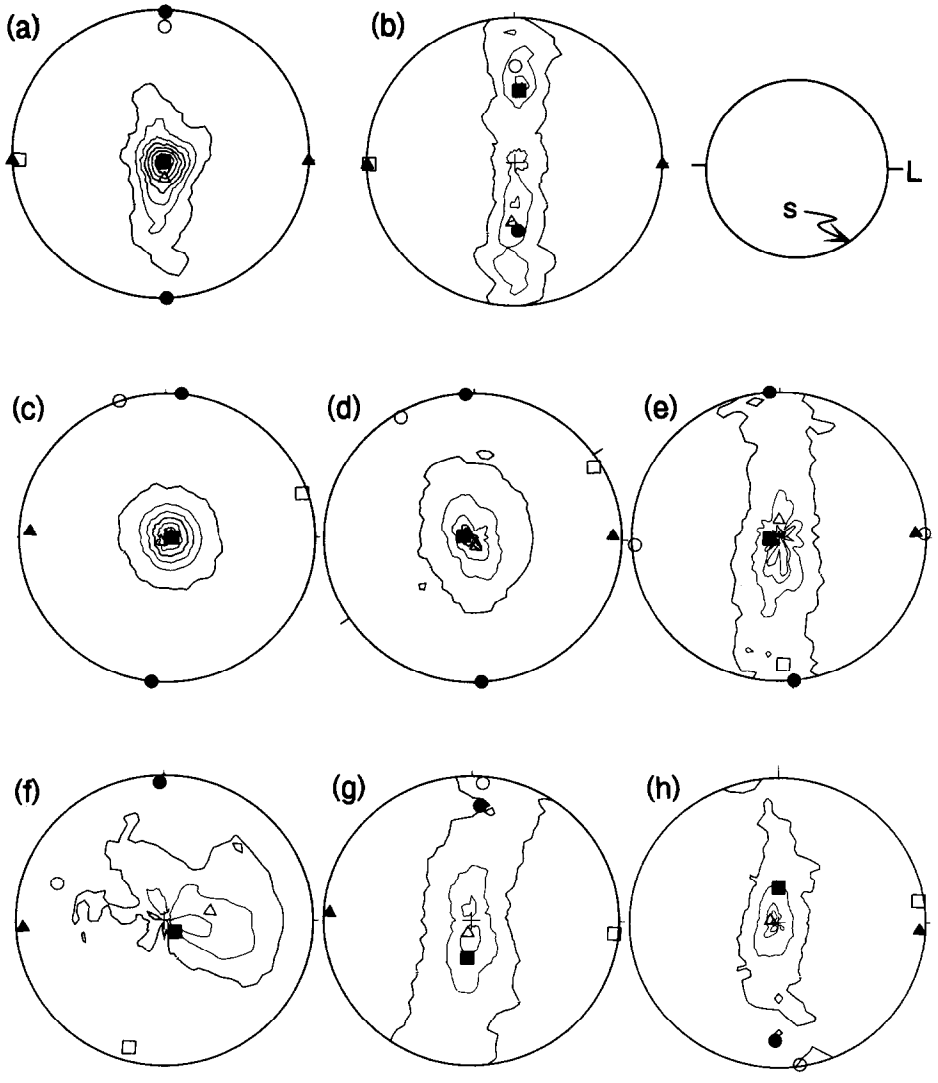

Fig. 3. Mica (001) preferred orientation patterns (muscovite or biotite) of the studied samples. (a) OG23, (b) OG25, (c) W96, (d) W41, (e) W13, (f) SZ12, (g) SZ21, (h) SZ41. Projection plane is the foliation S, the stretching lineation L strikes E–W, except for sample W41 where the results are given with respect to a weak mineral lineation. The orientation of the principal axes of the AMS tensor $\vec{K}_{max}$ (triangles), $\vec{K}_{int}$ (dots) and $\vec{K}_{min}$ (squares) is given by the filled symbols. Open symbols correspond to the axes of the orientation tensor ($\vec{e}_{min}$, $\vec{e}_{int}$, $\vec{e}_{max}$), which parallels the axes of the modelled AMS tensor (see text for details).

mica-rich surfaces. The criterion by which these samples were selected is the difference in the shape of the pole figure tensors, ranging from oblate (sample W96, T_{mica} = 0.90) to neutral shape (sample W13, T_{mica} = 0.02).

RESULTS

Texture

The observed orientation patterns of mica (001) poles (Fig. 3) vary from approximately perfect axial symmetry with a strong point maximum (sample W96, T_{mica} = 0.90, see Fig. 3c) to approximately complete girdles around the lineation containing several submaxima (sample OG25, T_{mica} = −0.95, Fig. 3b). The symmetry of the intensity distributions is mostly orthorhombic with a maximum close to the foliation pole. However, the intensity maximum on the complete girdle of sample OG25 departs about 45° from the foliation pole, and a bimodal maxima distribution with maxima of different intensity level is observed corresponding to the intense microfolding, which is characteristic for this sample (Siegesmund *et al.* 1993). Due to the observed intensity distribution, $\vec{e}_{max}$ does not fit the foliation pole, but departs by about 30° (Fig. 3b). In the relatively undeformed metagranitoid (SZ12) all axes $\vec{e}_i$ of the pole figure tensor depart from the axes of the external reference frame (Fig. 3f). For this sample only a weak preferred orientation was measured, and the symmetry of the intensity distribution is difficult to detect. Considering the relatively large grain size of quartz, plagioclase and K-feldspar and inhomogeneities in mineral distribution, large experimental errors of the pole figure measurement had to be accepted.

AMS

The measured bulk susceptibilities $\bar{K}_{exp}$ cover the range from 46 × 10^{-6}[SI] to 284 × 10^{-6}[SI], modelled

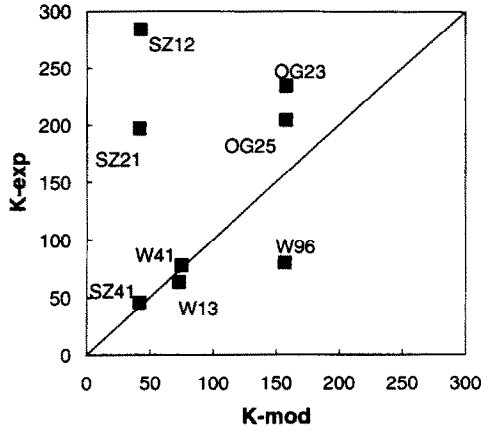

Fig. 4. Comparison between experimentally determined bulk rock susceptibilities (K_{exp}) and those modelled from modal composition and texture (K_{mod}).

bulk susceptibilities $\bar{K}_{mod}$ range from 42×10^{-6}[SI] to 158×10^{-6}[SI] and deviate from the experimental results (Fig. 4). All the investigated samples exhibit a pronounced AMS, in which the shape parameter T and the anisotropy degree P' also cover a wide range (Fig. 5). P' varies from 1.03 to 1.42, the shape parameter T from +0.95 (almost perfectly oblate, sample W96) to −0.72 (pronounced prolate, sample OG25). From the magnitude $\bar{K}$ of magnetic susceptibility, phyllosilicates may be assumed to be the main source of AMS.

In the orthogneiss samples, $\bar{K}_{exp}$ and $\bar{K}_{mod}$ moderately deviate from each other. The measured and modelled tensor agree well in orientation, with $\vec{K}_{max}$ and $\vec{e}_{min}$ exactly parallel to the stretching direction (Figs. 3a & b), i.e. they are also coaxial to the crenulation axes of the microfolds in sample OG25. In sample OG23, the magnetic foliation parallels the macroscopic foliation and in sample OG25 it is rotated by about 45°, with $\vec{K}_{min}$ and $\vec{K}_{int}$ corresponding to the submaxima in the pole figure.

In the granulites, a good conformity of $\bar{K}_{exp}$ and $\bar{K}_{mod}$ is observed, except in sample W96 where the modelled susceptibility is significantly higher. Generally, the pole of the magnetic foliation $\vec{K}_{min}$ lies very close to the pole of the mylonitic foliation; the angular distance between an individual measurement and the calculated mean value is <3°. In contrast, $\vec{K}_{max}$ and $\vec{K}_{int}$ show a different behaviour. In sample W96, the scatter of these vectors (four measured cores) is about ±20° in the magnetic foliation plane with the mean value of $\vec{K}_{max}$ close to the stretching direction, which was deduced from the c-axes maximum of prismatic sillimanite. Such a spread is also observed for sample W41 (four measured cores), but it is much smaller (±12°). In sample W13 (three measured cores), all principal directions of the AMS tensor form clusters. These observations can be related directly to the shape parameter T of the tensors. As for $T = +1$, no preferred orientation of $\vec{K}_{max}$ and $\vec{K}_{int}$ in the magnetic foliation is defined. Such a large spread of the tensor orientation for shape parameters close to +1, a decrease of this spread with decreasing T, and clustering for $T \approx 0$ can be expected.

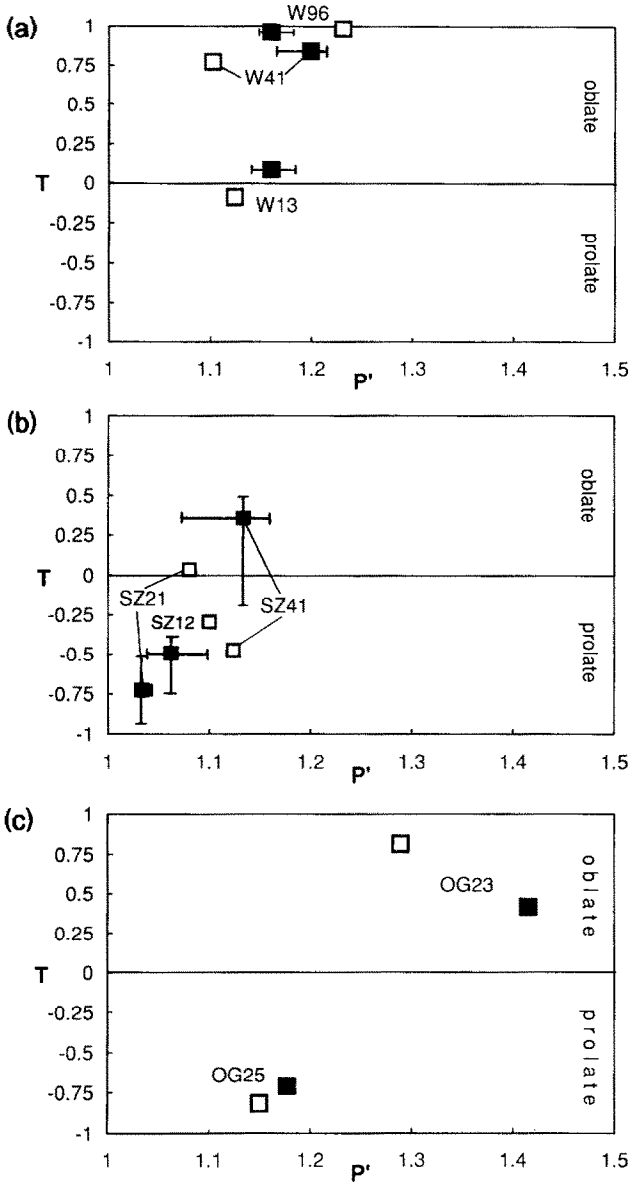

Fig. 5. Relationship between the anisotropy degree (P') and the shape parameter T of (a) granulites, (b) mylonites and (c) orthogneisses. Filled symbols refer to experimental data, open symbols to calculated data. Mean values are given and maximal deviations are indicated by a bar, except for the orthogneisses.

The orientation of the modelled tensors deviates from the orientation of the measured ones in a different way. In sample W13, it is slightly rotated around the stretching direction which parallels $\vec{K}_{max}$ (Fig. 3e). In the samples W41 and W96 it is rotated around the foliation pole ($\vec{K}_{min}$) by about 35° or 20°, respectively. The same can be stated about the shape and the anisotropy of the AMS tensors, where the corresponding parameters show moderate deviations. The greatest differences must be noted for P' of sample W41, where the measured value is significantly higher than the calculated one. The variation of individual measurements, which is given by the maximum deviation from the calculated mean values of T and P' is small, but the modelled values generally lie outside this range (Fig. 5a).

The rocks from the progressively deformed shear

zone generally exhibit large differences in $\bar{K}_{exp}$ and $\bar{K}_{mod}$. Only in sample SZ41 do these parameters agree well. Extreme differences are observed especially for sample SZ12. In all the samples the experimentally determined magnetic lineation $\vec{K}_{max}$ parallels the macroscopic lineation and the magnetic foliation is subparallel to the mesoscopic foliation. For samples SZ21 and SZ41 a good conformity with the modelled tensor is observed, but for sample SZ12 the orientation difference is significant.

Large deviations of the modelled and measured T and P' parameters are observed in nearly all cases (Figs. 3f–h). Whereas T and P' of sample SZ12 are rather close together, a significant difference in T must be noted for samples SZ21 and SZ41. For sample SZ21, a pronounced prolate shape of the tensor was measured, whereas the modelled tensor has a neutral shape. In sample SZ41 the experimentally determined tensor is moderately oblate, the modelled one moderately prolate. The variation of individual measurements is great, and this is valid for T and P' as well (Fig. 5b). Nevertheless, only the modelled P' of sample SZ41 lies inside the range indicating maximum deviation.

DISCUSSION

Relation between experimental and modelled AMS

Considering the obtained results for some samples, a rather good agreement was observed between the experimental and modelled AMS, but in some cases significant differences were found. The greatest differences of T are found in the samples from the progressive mylonite sequence and for sample OG23, where great differences of P' are observed as well. Several reasons can be given for the observed deviations, e.g. inaccurate determination or inhomogeneity of rock composition or errors during texture determination. Alternatively, the used single crystal data are not valid.

The variation of rock composition mainly influences the magnitude of $\bar{K}_{rock}$, and the greatest effect must be due to inaccurate determination of the volume fraction of mica minerals, or the presence of ore minerals with high volume susceptibility. To obtain a quantitative insight into the possible errors, $\bar{K}_{exp} = \bar{K}_{mod}$ was predetermined and recalculated for the required volume fraction of mica as well as the required amount of isotropic ilmenite, which are necessary to fulfil this condition. The volume susceptibility $\bar{K}$ of ilmenite was assumed to be 6000×10^{-6}[SI], and the rock composition was normalized by distributing the changes to the isotropic phases.

The recalculated volume fractions of mica and ilmenite are given in Table 3 in comparison with $\bar{K}_{exp}$ and $\bar{K}_{mod}$. In the case $\bar{K}_{exp} \approx \bar{K}_{mod}$ (samples W13, W41 and SZ41) the observed small changes in mica content may be explained by the inaccuracy of quantitative phase analysis, but for the samples OG23, OG25 and W96 large errors were assumed to explain the observed differences only by variation of the mica content. Such a correction is not possible for the samples SZ12 and SZ21, because the required mica volume fraction is >100%. On the other hand, additional ilmenite also corrects the observed differences of $\bar{K}_{exp}$ and $\bar{K}_{mod}$ (OG23: 1.3%, OG25: 0.8%, SZ12: 4.0%, SZ21: 2.6%), but this correction is not valid for W96 because $\bar{K}_{exp} < \bar{K}_{mod}$. The theoretical character of this kind of correction is confirmed by the fact, that no ilmenite could be observed in thin sections, but high values of $\bar{K}_{exp}$ may also be explained by small amounts of magnetite (≪1%) with very high volume susceptibility $\bar{K}$, which is difficult to detect in thin sections.

Table 3. The possible effect of a variation in the modal portion of mica and ilmenite to explain the observed deviations between the experimental and modelled mean susceptibility

Sample	K		Volume fraction	
	Experiment	Model	Mica	Ilmenite
OG23	234	158	20(14)	1.3
OG25	204	158	18(14)	0.8
W13	62	73	6 (7)	
W41	77	74	7 (7)	<0.1
W96	81	158	8(14)	
SZ12	284	42	>100(32)	4.0
SZ21	197	42	>100(32)	2.6
SZ41	46	42	34(32)	<0.1

To gain more information about the effect of varying phyllosilicate content on AMS, three samples characterized by different types of texture were selected (W96, OG25 and W13) as examples used in modelling the AMS for decreasing muscovite and biotite volume fractions. The remaining volume was assumed to consist only of quartz. The dependence of P' on the mica content is given for biotite in Fig. 6a and for muscovite in Fig. 6b together with the curves for the single crystals, which correspond to a perfect alignment of the (001) poles in a polycrystal. Changes of T are minimal and are not displayed graphically. With decreasing mica content, P' increases. This effect is more pronounced in the case of muscovite than in the case of biotite due to the postulated single crystal parameters. For this mineral an exchange of the tensor from prolate to oblate shape (OG25) or from oblate to prolate shape (W13, W96) occurs in the range from 5% to 10%. For volume fractions <5%, P' decreases. Due to the much higher anisotropy of biotite this change occurs at a volume content of <2%. The switch from oblate to prolate or vice versa is a consequence of opposite polarity of the magnetic vectors in diamagnetic and paramagnetic minerals. Starting with a tensor corresponding to a mica content of 100% and continuously replacing mica by isotropic quartz, the length of all the axes of the bulk AMS tensor is reduced by the same quantity. At a certain quartz content the length of the shortest axis $\vec{K}_{min}$ becomes zero, changes its polarity and then increases. The switch from prolate to oblate or reverse occurs when $\vec{K}_{int}$ also changes its polarity. Thus, very different values for T and P' are possible for a difference in mica content of a few volume percent as can often be observed in gneissic rocks.

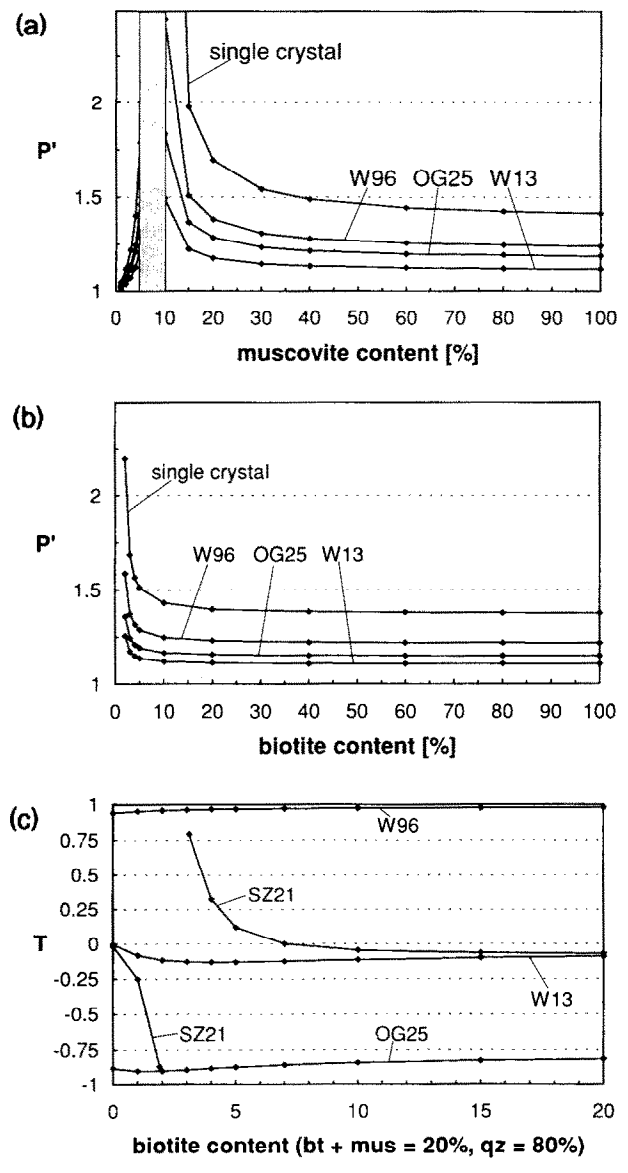

Fig. 6. Calculated variation of P' dependence upon mica content assuming biotite (a) and muscovite (b) to be the only phyllosilicate phase present. Three samples with quite different textures and shape parameters T were selected to demonstrate this interdependence. Additionally, the curves for the single crystals (corresponding to a textured polycrystal with perfect parallel alignment of the basal plane normals) are given. The remaining sample volume is assumed to be (isotropic) quartz. At a muscovite content in the range of 5%–10% (marked by a vertical bar) a switch of T from prolate to oblate shape or vice versa is observed. In the case of biotite this switch takes place at a volume fraction <2%, and is not displayed graphically. (c) Calculated variation of the shape parameter T dependent on the variable biotite/muscovite ratios (biotite + muscovite = 20%, quartz = 80%). Four samples were selected for demonstration. In the cases of W96, W13 and OG25 only small changes are observed, whereas SZ21 shows greater changes in T and a switch from prolate to oblate shape.

A more complex situation is observed in a three-phase system containing two anisotropic phases, biotite and muscovite (Fig. 6c), and considering the changes of T. The volume ratio of biotite and muscovite has been changed according to $V_{bt} + V_{mus} = 20\%$, the remaining volume fraction again is quartz. For the above selected samples W96, OG25 and W13 no extreme change of T is observed, except for sample SZ21 (Fig. 6c). With decreasing biotite content, T increases and a switch to prolate shape occurs in the range between 2% and 3%. Further decrease of the biotite content results in an increase of T. The only difference with respect to the other three samples is the type of texture, so it must be concluded that for specific texture types, great variations of T are possible independent of the volume ratio of the present anisotropic phases.

Relation to strain

Due to the tabular appearance of mica minerals the (001) pole figures contain information about planar fabric elements. This may be inferred from the predominant reorientation mechanism, which is grain shape controlled (e.g. Oertel 1983, 1985). In most cases the pole figures show a maximum parallel to the foliation pole, and additionally a more or less pronounced tendency to form a girdle around the stretching direction. Only in rare cases is this tendency not significantly developed.

The AMS tensor in low-susceptible rocks is closely related to the orientation tensor which is derived from the phyllosilicate (001) texture. Both the shape of the AMS tensor and the phyllosilicate texture depends on strain. This was the motivation for attempting to quantify finite strain from magnetic fabrics (e.g. Wood *et al.* 1976, Kligfield *et al.* 1977, Rathore & Hugan 1987). Various mathematical approaches based on the March model were realized (e.g. Hrouda 1987, Henry & Hrouda 1989). However, experimental studies demonstrated a change of AMS with increasing strain lacking a direct correlation between strain and AMS (e.g. Borradaile & Alford 1987). Most of these studies focused primarily on very low-grade shales and slates, where strain calculations from AMS were calibrated with the results of strain estimations using classical methods.

O'Brien *et al.* (1987) reported the development of a biotite preferred orientation in a progressively deformed granodiorite from the Santa Rosa mylonite zone, California. Increasing deformation is indicated by the (001) pole figure maximum, which increases from 2 m.r.d. in the weakly deformed granodiorite to 10 m.r.d. in the strongly deformed phyllonite. The bulk mineralogical composition remains unchanged during progressive deformation (10% biotite, 9% K-feldspar, 55% plagioclase and 26% quartz, see Wenk & Pannetier 1990) and for this composition, the AMS was calculated for a model rock based on biotite basal plane pole figures measured by neutron diffraction (Höfler 1989). The results of the modelling show an increase of T from moderately oblate shape ($T = 0.286$) to nearly perfect oblate shape ($T = 0.924$, see Fig. 7). P', which is a qualitative measure of strain, increases from 1.056 to 1.207 independent of the intensity of the pole figure maximum. The March strains calculated from a number of highly strained phyllonites from the Santa Rosa mylonite zone are more or less similar and low (O'Brien *et al.* 1987). From this observation it was concluded that mica-preferred orientations come to a stage of saturation and represent something like a steady-state fabric

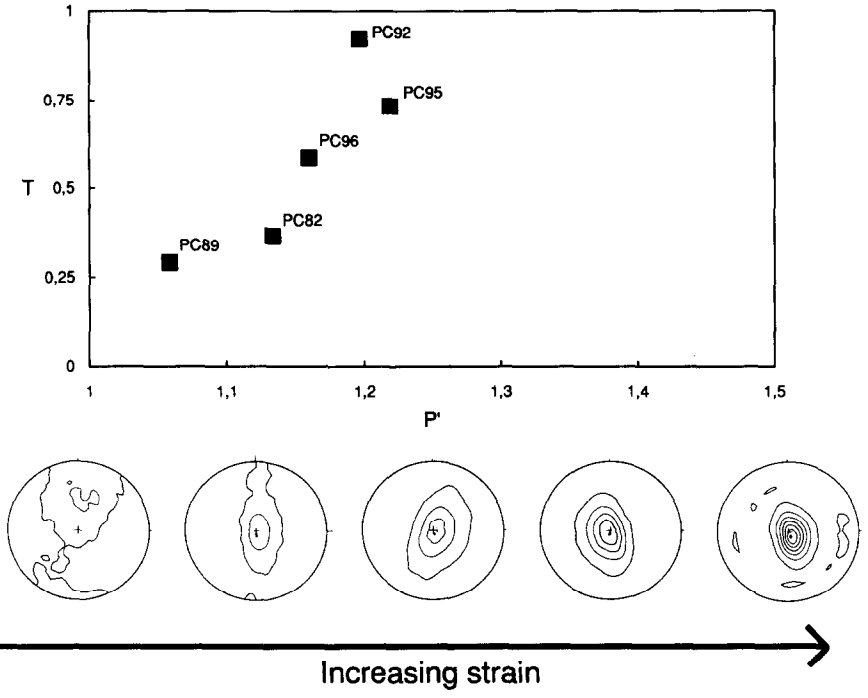

Fig. 7. P'/T diagram and biotite (001) pole figures for a sequence of progressively deformed samples from the Santa Rosa mylonite zone (PC89: weakly deformed protolith, PC92: ultramylonitic phyllonite). Increasing strain leads to a nearly axialsymmetric intensity distribution in the pole figures and a nearly perfect oblate shape of the calculated AMS ellipsoid. Note that P' increases upon the magnitude of strain.

comparable to the 'steady-state foliation' described by Means (1981); both the orientation tensor and the AMS tensor give only a lower limit of the magnitude of bulk strain. On the other hand, from the increase of P' for less deformed samples it may be assumed that in the case of weak deformation, strain estimates are in principle possible.

The above considerations are valid in the case of homogeneous and coaxial deformation as supposed by the March model, but there is evidence that deformation generally is inhomogeneous from the outcrop scale to the microscale. Various fabric elements are described which may influence the texture development of each phase in different ways (e.g. Berthe *et al.* 1979, Platt & Vissers 1980). O'Brien *et al.* (1987) found a significant influence of extensional cleavage planes on mica-preferred orientation. Furthermore, similar phyllosilicate-preferred orientations may originate in different strain regimes (Ullemeyer & Weber 1993). For example, quartz/feldspar rods may control the arrangement of phyllosilicates leading to an anastomosing schistosity and partial girdles in mica (001) pole figures. This is independent from the type of strain because rods may originate in each deformation regime producing a final strain ellipsoid with different lengths of its principal axes. Theoretically, in the case of cylindrical rods resulting from axial symmetric extension (prolate strain) complete girdles should be observed, whereas an additional flattening component causes flattened rods and incomplete mica (001) girdles (Fig. 8a). Extensional microshear planes resulting from triaxial pure shear with shortening normal to the foliation and extension parallel to the foliation may also generate partial girdles (Fig. 8b). Coaxial pure strain with shortening parallel to the foliation leading to compressive crenulation as observed during folding of rocks (see sample OG25 as an example) may be a further possibility to generate phyllosilicate girdles (Fig. 8c). Since these controlling mecha-

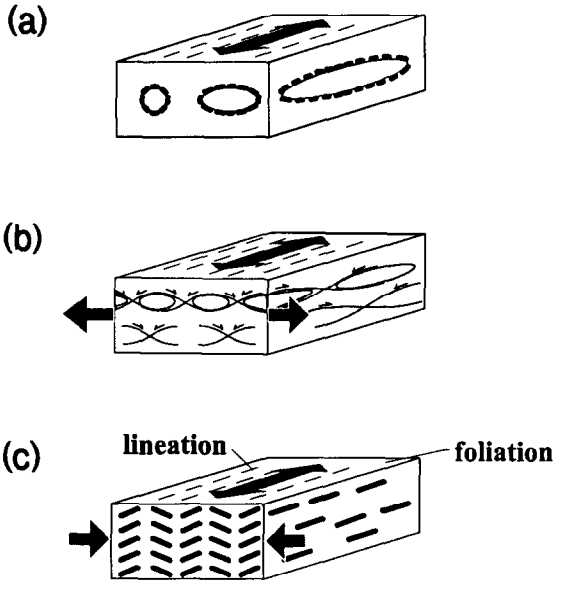

Fig. 8. Models to explain the origin of phyllosilicate (001) partial girdles in strained rocks with pronounced extension parallel L (from Ullemeyer & Weber 1993). (a) Mica preferred orientation is controlled by inhomogeneities (e.g. oblate or prolate quartz/feldspar aggregates) leading to an anastomosing schistosity. (b) Arrangement of the mica flakes on micro shear planes caused by an extensional deformation component perpendicular L (oblate strain). Extensional shear planes may be genetically connected to inhomogeneities in mineral distribution. (c) Crenulation due to shortening parallel L (prolate strain).

nisms may act simultaneously, no simple relationship between the type and magnitude of strain exists.

CONCLUSIONS

In this study, the AMS of polyphase-deformed metamorphic rocks was measured and compared with the results of modelling, based on the texture of the anisotropic rock components and the modal composition of the rock. The orientation of the AMS ellipsoid generally corresponds well to rock fabrics and may be explained by (001) mica-preferred orientation. On the other hand, experimental and computed values of $\bar{K}$, P' and T do not agree very well. The observed deviations are significant and it must therefore be concluded, that AMS does not depend exclusively on the texture of paramagnetic rock constituents. From the observation that for several samples $\bar{K}_{exp}$ is much larger than $\bar{K}_{mod}$, it is inferred that accessory ferromagnetic minerals are also a controlling factor of rock AMS. $\bar{K}_{mod}$ can be adjusted to $\bar{K}_{exp}$ by adding small amounts of ilmenite or very small amounts of magnetite. Such an adjustment is not possible for sample W96 (because $\bar{K}_{exp} < \bar{K}_{mod}$), but can be done by the reduction of the volume fraction of mica. Increase of the mica fraction also corrects $\bar{K}_{mod}$ (samples OG23 and OG25), but the required changes of the mica volume fraction are particularly large and possibly indicate large errors of quantitative phase analysis. The conclusion reached is, that an accurate phase analysis is one premise for the modelling of AMS, especially the identification of high susceptible phases. Since the ferromagnetic contribution to bulk rock AMS may in principle also be separated experimentally (Hrouda & Jelinek 1990), it might be beneficial to compare the results obtained from modelling with an experimental AMS, which is corrected for its ferromagnetic component as proposed above. Such a comparison may also be used to test, if modelling allows, the separation of the ferromagnetic part of the whole rock AMS.

The AMS of rocks containing only small volume fractions of mica may be characterized by extreme variations of P' and/or T, as could be demonstrated for model rocks containing one or two paramagnetic phases with different single-crystal anisotropies. In the system containing one paramagnetic phase the changes of T are small, but a sudden switch from oblate to prolate shape (or reverse) of the AMS tensor occurs in all cases. This effect, which is texture independent and valid only for small mica volume fractions, demonstrates the influence of the diamagnetic rock constituents with opposite polarity of its magnetic vectors. Such an effect does not occur in the case of identical magnetic polarization of all phases. Furthermore, the type of texture may also have some influence on whole rock AMS. In sample SZ21, T depends on the ratio of biotite and muscovite, i.e. the shape of the bulk tensor resulting from the contributions of two anisotropic phases with different single crystal anisotropies (biotite and muscovite) and one diamagnetic phase (quartz).

The large spread of individual measurements of the samples SZ12, SZ21 and SZ41 indicates, that AMS may also be unevenly distributed in hand specimen. Since T_{mod} and T_{exp} are extremely different and T_{mod} never fits the interval defined by the individual measurements, it is assumed, that the used model texture is not representative for the characterization of the shape of the bulk AMS tensor.

The observation that the magnetic fabric (magnetic lineation, magnetic foliation) coincides with the rock fabric does not support any strain correlation. The output of the AMS must be considered to be a weighted total of all superposed microfabrics, which may generate in different strain regimes and often cause a lowering of symmetry in the mica pole figures, that cannot be described by the highly symmetrical AMS tensor. Therefore, the AMS cannot replace texture analysis, or be an alternative approach to such an analysis as was recently suggested by Borradaile (1991). The simple AMS versus strain versus texture correlation is not valid.

Acknowledgements—We are grateful for the stimulating discussions with F. Hrouda, A. Vollbrecht, B. van der Pluijm and K. Weber. S. Höfler and W. Schäfer provided us the neutron diffraction data from the Santa Rosa mylonite zone and Z. Pros the orthogneiss samples. Technical help was provided by B. Mackewic, Ch. Groß and T. Weiß. This research project was supported by the Deutsche Forschungsgemeinschaft.

REFERENCES

Adam, J. 1989. Methoden und Algorithmen zur Verwaltung und Analyse axialer 3-D-Richtungsdaten und ihrer Belegungsdichten. *Göttinger Arb. Geol. Paläont.* **40**, 1–100.

Bartosek, J., Jelinek, V. & Pros, Z. 1985. Comparison of elastic and magnetic anisotropies of two types of metamorphosed rocks demonstrated on spherical specimens. In *Physical Properties of the Mineral System of the Earth's Interior* (edited by A. Kapicka, V. Kropacek & Z. Pros). (CAPG-Project 3) 59–64.

Borradaile, G. 1987. Anistropy of magnetic susceptibility: rock composition versus strain. *Tectonophysics* **138**, 327–329.

Borradaile, G. 1988. Magnetic susceptibility, petrofabric and strain—a review. *Tectonophysics* **156**, 1–20.

Borradaile, G. 1991. Correlation of strain with anisotropy of magnetic susceptibility (AMS). *Pure & Appl. Geophys.* **135**, 15–29.

Borradaile, G. J. & Alford, C. 1987. Relationship between magnetic susceptibility and strain in laboratory experiments. *Tectonophysics*, **133**, 121–135.

Borradaile, G., Keeler, W., Alford, C. & Sarvas, P. 1987. Anisotropy of magnetic susceptibility of some metamorphic minerals. *Phys. Earth & Planet. Interiors* **172**, 215–222.

Bunge, H. J. 1982. *Texture Analysis in Materials Sciences*. Butterworth, London.

Compagnoni, R. 1977. The Sesia-Zone: high pressure/low temperature metamorphism in the Australoalpine Continentale Margin. *Rendiconti Soc. Italiano di Mineral. e Petrol.* **33**, 335–374.

Finke, W. 1910. Magnetische Messungen an Platinmetallen und monoklinen Kristallen insbesondere der Eisen-, Kobalt- und Nickelsalze. *Ann. Physik.* **31**, 149–168.

Henry, B. & Hrouda, F. 1989. Analyse de deformation finite des roche par determination de leur anisotropie desusceptibilite magnetique. *C.R. Acad. Sci. Paris, s II* **308**, 731–737.

Höfler, S. 1989. Texturanalyse an Metallen und Mineralien und Bestimmung von Meteorit-Mikrostrukturen mit Neutronenbeugung. Berichte der Kernforschungsanlage Jülich, Nr. 2274, Ph.D. thesis.

Hrouda, F. 1982. Magnetic anisotropy of rocks and its application in geology and geophysics. *Geophys. Surv.* **5**, 37–82.

Hrouda, F. 1986. The effect of quartz on the magnetic anisotropy of quartzite. *Stud. Geophys. Geodet.* **30**, 39–45.

Hrouda, F. 1987. Mathematical model relationship between the paramagnetic anisotropy and strain in slates. *Tectonophysics* **142**, 323–327.

Hrouda, F. & Jelinek, V. 1990. Resolution of ferrimagnetic and paramagnetic anisotropies in rocks, using combined low-field and high-field measurements. *Int. J. Geophys.* **103**, 75–84.

Hrouda, F., Siemes, H., Herres, N. & Hennig-Michaeli, C. 1985. The relationship between the magnetic anisotropy and the c-axis fabric in a massive hematite ore. *J. Geophys.* **56**, 174–182.

Hrouda, F. & Schulmann, K. 1990. Conversion of magnetic susceptibility tensor into orientation tensor in some rocks. *Phys. Earth & Planet. Interiors* **63**, 71–77.

Isler, A. & Zingg, A. 1974. Geologie der Sesia Zone zwischen Rimella und der Valle Anzasca (Norditalien). *Schweiz. miner. petrogr. Mitt.* **54**, 81–97.

Jelinek, V. 1977. The statistical theory of measuring anisotropy of magnetic susceptibility of rocks and its application. Geofizika Brno.

Jelinek, V. 1981. Characterization of magnetic fabric of rocks. *Tectonophysics* **79**, 563–567.

Juckenack, Chr. 1990. Beitrag der Anisotropie der magnetischen Suszeptibilität (AMS) für Struktur- und Gefügeuntersuchungen von Metamorphiten: Einzelbeispiele und regionale Anwendung im Spessart-Kristallin. Ph.D. Thesis, University of Göttingen.

Kligfield, R., Lowrie, W. & Dalziel, A. W. D. 1977. Magnetic susceptibility anisotropy as a strain indicator in the Sudbury Basin, Ontario. *Tectonophysics*, **40**, 287–308.

Means, W. D. 1981. The concept of steady-state foliation. *Tectonophysics*, **78**, 179–199.

O'Brien, D. K., Wenk, H.-R., Ratschbacher, L. & You, Z. 1987. Preferred orientation of phyllosilicates in phyllonites and ultramylonites. *J. Struct. Geol*, **9**, 719–730.

Oertel, G. 1983. The relationship of strain and preferred orientation of phyllosilicate grains in rocks—a review. *Tectonophysics* **100**, 413–447.

Oertel, G. 1985. Reorientation due to grain shape. In: *Preferred Orientation in Deformed Metals and Rocks: An Introduction to Modern Texture Analysis* (edited by Wenk, H.-R.). Academic Press Inc., Orlando, Florida, 259–265.

Owens, W. H. & Rutter, E. H. 1978. The development of magnetic susceptibility anisotropy through crystallographic preferred orientation in a calcite rock. *Phys. Earth & Planet. Interiors* **16**, 215–222.

Platt, J. P. & Vissers, R. L. M. 1980. Extensional structures in anisotropic rocks. *J. Struct. Geol.* **2**, 397–410.

Rathore, J. S. & Hugon, H. 1987. Comparison of magnetic, mica and reduction spot fabrics in the Rocroi Massiv, Ardennes, Frances. In: *The Rhenish Massif* (edited by Vogel, A., Miller, H. & Greiling, R.). Vieweg, Barunschweig, 79–94.

Richter, C., van der Pluijm & Housen, B. A. 1993. The quantification of crystallographic-preferred orientation using magnetic anisotropy. *J. Struct. Geol.* **15**, 113–116.

Richter, C., Ratschbacher, L. & Frisch, W. 1993. Magnetic fabrics, crystallographic-preferred orientation, and strain of progressively metamorphosed pelites in the Helvetic zone of the Central Alps (Quartenschiefer Formation). *J. geophys. Res.* **98, No. B6**, 9557–9570.

Rochette, P. 1987. Magnetic susceptibility of the rock matrix related to magnetic fabric studies. *J. Struct. Geol.* **9**, 1015–1020.

Scheidegger, A. E. 1965. *On the Statistics of the Orientation of Bedding Planes, Grain Axes, and Similar Sedimentological Data. U.S. G.S. Prof. Paper*, **525C**: 164–167.

Siegesmund, S. 1995. The significance of rock fabrics for the geological interpretation of geophysical anisotropies. *Geotekt. Forsch.* (in press).

Siegesmund, S. & Dahms, M. (1994). Fabric-controlled anisotropy of elastic, magnetic and thermal properties of rocks. In: *Textures of Geological Materials* (edited by Bunge, H.-J., Siegesmund, S., Skrotzki, W. & Weber, K). Deutsche Gesellschaft für Materialkunde-Verlag, 353–380.

Siegesmund, S., Vollbrecht, A., Chlupac, T., Nover, G., Dürrast, H., Müller, J. & Weber, K. 1993. Fabric-controlled anisotropy of petrophysical properties observed in KTB core samples. *Sci. Drilling* **4**, 31–54.

Siegesmund, S., Vollbrecht, A. & Pros, Z. 1993. Fabric changes and their influence on P-wave velocity patterns-examples from a polyphase deformed orthogneiss. *Tectonophysics*, **225**, 447–492.

Sintubin, M. 1994. Texture types in shales and slates. In: *Textures of Geological Materials* (edited by Bunge, H.-J., Siegesmund, S., Skrotzki, W. & Weber, K.). Deutsche Gesellschaft für Materialkunde-Verlag, 221–230.

Ullemeyer, K. 1992. Methodische Untersuchungen zur Röntgentexturanalyse und Gefügeuntersuchungen an Granuliten der Südlichen Böhmischen Masse. Ph.D. thesis, University of Göttingen.

Ullemeyer, K. & Weber, K. 1993. Preferred orientation of phyllosilicates in mylonitic rocks and their implications for kinematic interpretation. *Fisika Semli* **6**, 104–112. (in Russian).

Ullemeyer, K. & Weber, K. 1994. Correction of phyllosilicate (002) X-ray pole figure measurements. In: *Textures of Geological Materials* (edited by Bunge, H.-J., Siegesmund, S., Skrotzki, W. & Weber, K.). Deutsche Gesellschaft für Materialkunde-Verlag, 83–91.

Uyeda, S., Fuller, M. D., Belshe, J. C. & Girdler, R. W. 1963. Anisotropy of magnetic susceptibility of rocks and minerals. *J. geophys. Res.* **68**, 279–291.

Weber, K. 1981. Kinematic and metamorphic aspects of cleavage formation in very-low grade metamorphic slates. *Tectonophysics* **78**, 291–306.

Weber, K. & Duyster, J. 1990. Moldanubian zone of the Waldviertel, Lower Austria. In: *IUGS-Conference on paleozoic orogens in Central Europe—Field Guide Bohemian Massif* (edited by Franke, W. & Weber, K.), 99–114.

Wenk, H.-R. & Pannetier, J. 1990. Texture development in deformed granodiorites from the Santa Rosa mylonite zone, Southern California. *J. Struct. Geol.* **12**, 177–184.

Williams, P. F. 1972. Development of metamorphic layering and cleavage in low grade metamorphic rocks at Bermagui, Australia. *Am. J. Sci.* **271**, 1–47.

Wood, D. S., Oertel, G., Singh, J. & Bennet, H. F. 1976. Strain and Anisotropy in rocks. *Philos. Trans. R. Soc. Lond.* **283**, 27–42.

Zapletal, K. 1990. Low-field susceptibility anisotropy of some biotite crystals. *Phys. Earth & Planet. Interiors* **63**, 8